

An analytical equation to predict mortar spalling at laboratory scale

Mendonça Filho, F. F.; de Vilder, L.; Schlangen, E.; Çopuroğlu, O.

DOI

[10.1016/j.conbuildmat.2024.136366](https://doi.org/10.1016/j.conbuildmat.2024.136366)

Publication date

2024

Document Version

Final published version

Published in

Construction and Building Materials

Citation (APA)

Mendonça Filho, F. F., de Vilder, L., Schlangen, E., & Çopuroğlu, O. (2024). An analytical equation to predict mortar spalling at laboratory scale. *Construction and Building Materials*, 428, Article 136366. <https://doi.org/10.1016/j.conbuildmat.2024.136366>

Important note

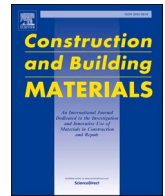
To cite this publication, please use the final published version (if applicable). Please check the document version above.

Copyright

Other than for strictly personal use, it is not permitted to download, forward or distribute the text or part of it, without the consent of the author(s) and/or copyright holder(s), unless the work is under an open content license such as Creative Commons.

Takedown policy

Please contact us and provide details if you believe this document breaches copyrights. We will remove access to the work immediately and investigate your claim.



An analytical equation to predict mortar spalling at laboratory scale

F.F. Mendonça Filho^{*}, L. de Vilder, E. Schlangen, O. Çopuroğlu

Materials & Environment, Faculty of Civil Engineering and Geosciences, Delft University of Technology, Stevinweg 1, Delft, Netherlands

ARTICLE INFO

Keywords:

Concrete spalling
Pore connectivity
Concrete fire damage
X-ray microtomography

ABSTRACT

Spalling is the main problem concerning safety in concrete structures under rapid heating. Despite being studied for nearly a century, its prediction remains a challenge. In addition, the main recommendations for its prevention are merely the addition of a fixed amount of polypropylene fibres, without accounting for mix design. This paper presents an experimental study focusing on the thermo-hygral mechanism contribution to spalling. The use of mercury intrusion porosimetry and X-ray microtomography for the determination of pore connectivity is considered a key parameter. The results of the experiment are used for the development and calibration of an analytical equation capable of predicting spalling in concrete samples. The equation is then validated using over 100 examples extracted from literature, achieving an accuracy of 91.2%. Based on the validation, the proposed equation is a step forward in the prediction of concrete spalling based on the mix design parameters.

1. Introduction

Residential fires still cost thousands of lives around the world annually [1]. The main strategy to avoid such losses is to design structural elements

capable of lasting long enough for safe evacuation [2]. While concrete structures are generally safer than steel against fire [3–5], spalling remains as the core disadvantage against safety in these structures under extreme heat. That is when pieces of material are violently propelled from structural members during rapid temperature increase [6]. In addition, while most durability problems can be addressed by the use of high performance concrete [7–10], the increase in concrete grade only exacerbates spalling

[11–13].

This phenomenon has been studied for decades [15–17], however, to date, predicting the fire resistance from the mix design and properties of a concrete remains a challenge [14]. Fire proofing technologies have been developed [18–20], but these are not mandatory and often prove themselves ineffective during field testing [21,22]. Therefore, the main focus should be on determining if the material itself will suffer from spalling. Yet, spalling is governed by the combination of two different mechanisms, occurring synchronously during a rise in temperature that changes the material composition and properties [23,24]. Because simultaneous changes occur during a non-equilibrium state, it is hard to establish a correlation between material properties and failure even in controlled laboratory settings.

The thermo-mechanical mechanism (TMM) of spalling has been studied the most as it is the oldest theory concerning fire damage in concrete [25]. This consists of high tensile stresses generated parallel to the heated face [26] (see Fig. 1, left) and it can be examined in concrete through experiments with dry samples, in which the thermo-hygral mechanism (THM) becomes negligible [27]. Further, while solid materials are also affected by this form of deterioration [28], the lack of pores reduces the problem to a pure thermo-mechanical damage event. In this case, damage can be predicted with reasonable accuracy using Eq. 1, proposed by Lu and Fleck [29], which assumes local spalling in a material as a crack formation in a finite thickness plate in contact with a convective medium of different temperature. In the mentioned research [29], the investigators consider cracking due to cold or hot damage for materials depending on toughness or tensile strength in four different equations. Eq. 1 regards hot shock in a brittle material, the case that best approaches cement based materials.

$$\Delta T = C_2 \cdot \frac{\sigma_f}{E \cdot \alpha} \cdot \frac{k}{h \cdot H} \quad (1)$$

In which ΔT is the maximum temperature gradient to which the material can be subjected without appreciable thermal damage (K), C_2 is a constant, σ_f is the tensile strength of the material (N/m^2), E is the elastic modulus (N/m^2), α is the coefficient of thermal expansion ($1/K$), k is the thermal conductivity ($W/m/K$), h is the heat transfer coefficient between the material and the medium ($W/m^2/K$) and H is the volume of the sample divided by the heated surface (m).

^{*} Corresponding author.

E-mail address: f.filho@tudelft.nl (F.F. Mendonça Filho).

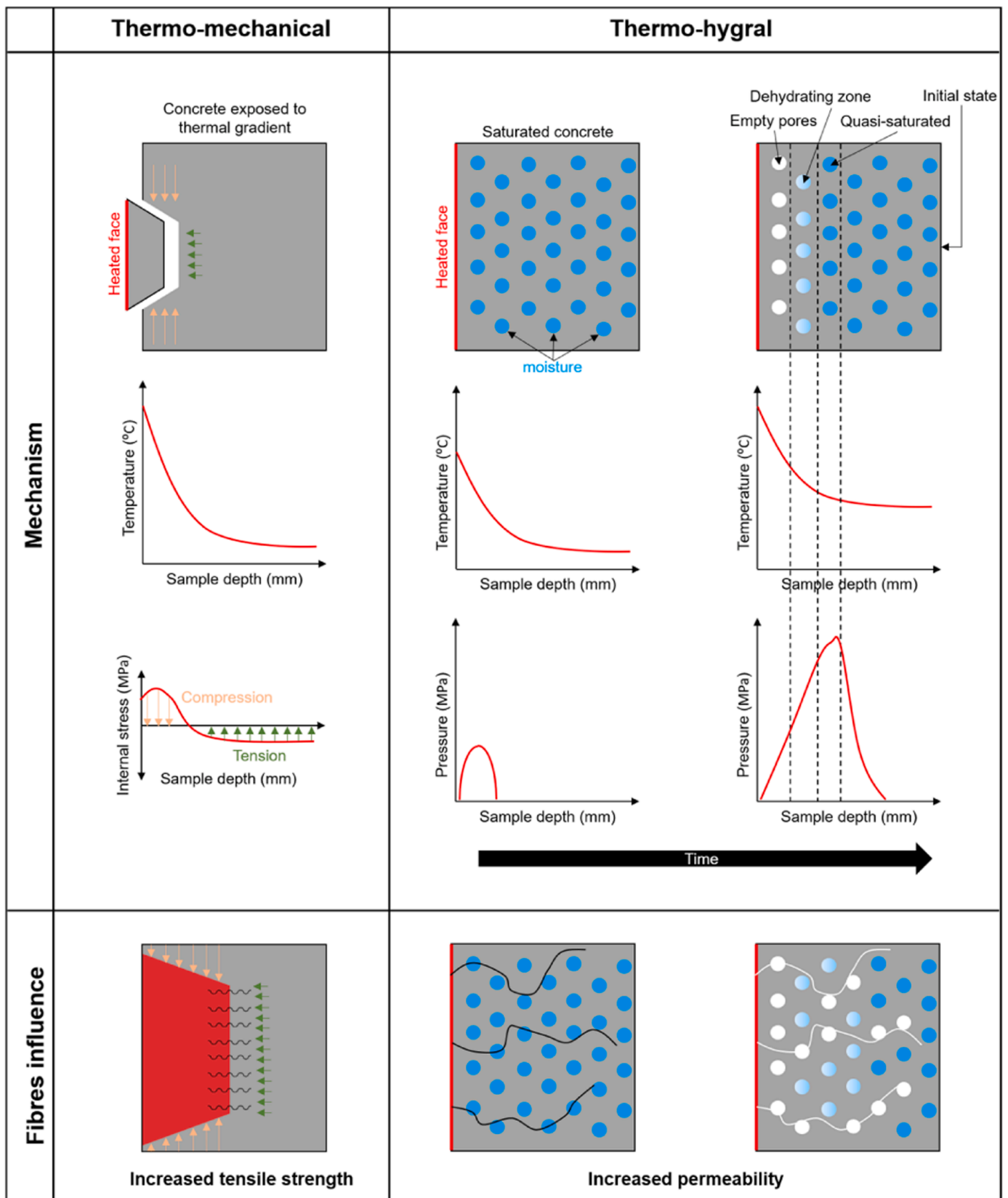


Fig. 1. Conceptual mechanisms responsible for high temperature spalling in concrete and the influence of fibres addition.

Table 1
Mixture proportions of cast samples.

Sample Name	C (kg)	W (kg)	A (kg)	SP (kg)	PP (%)	PPI* (-)
30_00	1	0.30	2	0.0059	0.00	0
30_05	1	0.30	2	0.0069	0.05	174
30_10	1	0.30	2	0.0094	0.10	348
40_00	1	0.40	2	0.0000	0.00	0
40_05	1	0.40	2	0.0000	0.05	174
40_10	1	0.40	2	0.0000	0.10	348
50_00	1	0.50	2	0.0000	0.00	0
50_05	1	0.50	2	0.0000	0.05	174
50_10	1	0.50	2	0.0000	0.10	348

C = cement, W = water, A = aggregates, SP = superplasticizer, PP = polypropylene fibres, PPI = polypropylene index.

* Calculated according to Li et al. (2021) [44], the definition of PP index is given in the Validation section.

On the other hand, the THM always suffers influence from thermo-mechanical stresses developed during heating [30,31], thus it cannot be studied individually [32]. This mechanism is attributed to the pressure build-up within saturated pores facing an advancing drying front caused by the heating of a concrete face [33], as depicted in Fig. 1, right. Because the pressure development within the material is inversely proportional to the maximum flow of water vapor, it is generally accepted that a more porous microstructure is less susceptible to this form of spalling [34]. Additionally, it has been shown that concrete with polypropylene fibres has increasing intrinsic permeability when heated [35], it is hypothesized that low melting temperature fibres leave channels increasing pore connectivity during concrete heating, facilitating vapor transport [36].

Moreover, different attempts were proposed to describe the phenomenon through finite element methods [37–40], including the combination of the above mentioned mechanisms via hygro-thermo-mechanical models. However, those are insensitive to mixture variations, using randomised concrete meso-structures. Other approaches [41,42], which take the material microstructure into account, still have problems estimating hygro-thermal contribution to the damage or the plain impact of polymeric fibres addition. This can be attributed to good comprehension of pore mechanics for individual pores, but poor understanding of the total pore pressure interaction with other parameters in the material [43]. Hence, a continuous effort of the experimental community in focusing on this variable for the spalling form of damage [45–48].

Recently Li et al. [44] produced a review on the advances and limitations of current methods studying pore pressures in concrete. However, pore dimensions span several orders of magnitude with different levels of saturation. Meanwhile, pressure measuring devices can only characterize small, punctual volumes in a sample. Consequently, no specific pore size or distribution correlation has been found as a clear indication of spalling resistance. In this paper, a question is posed if pore connectivity would be a better parameter for determining material resistance to spalling and further, if such connectivity can be engineered through mix design modifications.

The authors propose a method to minimize the effects of the TMM and focus on the study of the influence of mix design choices. Emphasis is given to the resistance against spalling caused predominantly by the THM. In particular the concept of pore connectivity and how this might be estimated at different scales is used. A combination of air content, mercury intrusion porosimetry (MIP) and X-ray computer microtomography (μ CT) is used to investigate the influence of the samples pore network in their response to spalling.

The results show a good correlation of the proposed connectivity measure to spalling resistance of samples. Based on these findings, the authors propose an analytical equation to predict the spalling or resistance of concrete to a given thermal load. The equation is validated using experiments from literature that include several cases outside of

the parameters tested in the experimental campaign.

2. Materials & methods

2.1. Mix design

All samples were cast as mortar using Portland cement type CEM I 42.5 N, tap water and CEN-Norm Sand with a distribution according to DIN EN 196–1 [49]. To achieve a difference in porosity and pore connectivity throughout the samples, the W/C ratio and polypropylene (pp) fibre content were varied. The fibres used were Fibermesh® 150, which were 12 mm in length and 31 μ m in diameter. Some mixtures presented poor workability, in which case MasterGlenium® 51 was used as superplasticizer.

A total of nine different mortar mix designs were selected (Table 1). The W/C ratio and fiber content (by volume) were increased between 0.30, 0.40 and 0.50 and 0.00%, 0.05% and 0.10%, respectively. For each mixture, five samples were cast in plastic cylinder moulds, with 65 mm height and 55 mm diameter. A cylindrical mould shape was chosen to highlight the contribution of the pore pressure build-up to the spalling behaviour of the samples, as edges are more prone to suffer from the TMM [32]. From the five cast samples of each mixture, three were used for spalling experiments, one for X-ray microtomography and one for mercury intrusion porosimetry. All samples were stored for 8 weeks in a fog room at 20 °C and >95% RH before testing. Additionally, each mixture also had three cubes with 40 mm sides and six prisms with 40 \times 40 mm cross section and 160 mm length cast for the mechanical testing. In Table 1, samples were labelled using the W/C ratio as the first value, and then the pp fibre content as the second value. E.g. 40_10 is a mix design with W/C ratio 0.40 and fibre content of 0.10%.

2.2. Heating experiment

Spalling tests were performed inside an open element HTF1700 Carbolite Furnace with an Eurotherm 3208 temperature controller. The oven possessed a base composed of refractory magnesia bricks where each sample would be placed and then covered by a hollow cylindrical steel cage to protect the exposed heating elements. The cage had multiple holes in all direction to allow heat flow through it. The refractory base had a much smaller thermal dilation than the samples and was considered inert for the duration of the experiment. For each mixture composition, three identical samples were tested. As the research focused on the thermos-hygral mechanism, the samples were tested in a saturated state.

Maximum oven temperature was set at 600 °C. Three different heating programs were used to test the samples. A heating rate of either 10, 30 or 50 °C/min was used, with a dwell time of 30 minutes. After remaining at maximum temperature for the duration of the dwell time, the oven would be turned off and the samples cooled gradually until an internal temperature under 40 °C, at which point the samples were removed from the oven for further study. In the case of spalling before the cooling phase, the program was interrupted and the oven turned off.

2.3. Mechanical properties

To determine compressive strength of each mixture, three cubes with 40 mm length were tested according to NEN-EN 12390–3:2019 [50]. The samples were tested after 28 days of curing at a fixed loading rate of 13.5 kN/s using a servo-hydraulic mechanical press with maximum load capacity of 5000 kN and high stability from Matest.

For determination of flexural strength, three prisms with a cross-section of 40 \times 40 mm and a length of 160 mm were tested for each mixture according to NEN-EN 12390–5:2019 [51]. The samples were tested after 28 days of curing, using a servo-hydraulic mechanical press with maximum load capacity of 5000 kN from Matest. The testing setup used a three point bending system with a centre top loading and two

rollers at the bottom with a spacing of 120 mm between them. Notches of 3 mm were introduced to the bottom in the middle of each sample to ensure cracking in the middle area. Two gauges were glued to both sides of the bottom of the samples to measure the strain. Testing was done with displacement control using the crack width monitored from the applied gauges.

Due to logistic issues, only six mixtures could have the Young's modulus tested. The tests were carried according to NEN-EN 12390-13:2021 [52]. Testing was loading-controlled with a loading rate of 0.1 kN per second (0.063 MPa/sec) using an Instron 8872. The stabilized secant modulus was measured after 3 load cycles with a maximum loading of 9 kN. Gauges were glued to all 4 sides of the samples with an initial length of 60 mm parallel to the vertical surface. Sandpaper was used to level the the top and bottom surface.

For each of the six tested mixtures, three prisms with a cross-section of 40 × 40 mm and a length of 160 mm were used. The three untested mixtures were 30_05, 40_05 and 50_05. To estimate elastic moduli of these mixtures, an average of the values of the other mixtures weighted by the flexural strength was used following Eq. 2.

$$E_{05} = \frac{\left(\frac{E_{00}}{f_{00}} + \frac{E_{10}}{f_{10}} \right)}{2} \cdot f_{05} \quad (2)$$

Where, E_{05} is the elastic modulus of a mixture with a fibre content of 0.05%, E_{00} is the elastic modulus of a mixture with a fibre content of 0.00%, E_{10} is the elastic modulus of a mixture with a fibre content of 0.10%, f_{00} is the flexural strength of a mixture with a fibre content of 0.00%, f_{05} is the flexural strength of a mixture with a fibre content of 0.05% and f_{10} is the flexural strength of a mixture with a fibre content of 0.10%.

2.4. Microstructure characterization

Air content tests were performed using a Form+Test Prufsysteme Air Entrainment Meter according to the standard NEN-EN 1015-7:1998 [53]. To prepare samples for mercury intrusion porosimetry, small pieces of samples were broken to a maximum size of 10 mm. Hydration was stopped using solvent exchange with isopropanol for 3 days and subsequently vacuum dried to remove the isopropanol for 2 days. The amount of time for stopping hydration was determined based on previous work [54]. MIP was performed using a Micromeritics AutoPore IV 9500 Mercury Porosimeter. A contact angle of 141 degrees was assumed. According to the minimum and maximum applied pressures of 345 KPa and 414 MPa, respectively, the porosimeter can analyze pores with apparent diameters of 100–0.006 μm . The pore connectivity was determined for the mortars using Eq. 3 from the work of Yu et al. (2018) [55].

$$\text{Pore connectivity (\%)} = \left(1 - \frac{\text{Ink - bottle porosity}}{\text{Total porosity}} \right) \cdot 100 \quad (3)$$

Samples were acquired for microtomography by coring a cylinder with a diameter of 12 mm out of the original cast cylinders. From the cored sample the middle section was selected with a height of 20 mm. After coring they were placed in a SECADOR desiccator to stop hydration. After 5 days in the desiccator the samples were submerged in a Kalium Iodine solution, to improve the contrast for the μCT images. The solution had a concentration of 0.05 M, all 9 samples were submerged in the solution and stored in airtight conditions for 2–3 days. After which, samples were removed from the solution and wrapped in plastic foil to retain the solution during the scans.

Microtomography scans were performed using a Phoenix Nanotom X-ray CT scanner. The scanner is composed of a transmission type X-ray tube, a sample stage and a 3072 × 2400 flat panel detector with a pixel size of 100 μm . The transmission target uses a tungsten filament and possesses a maximum accelerating voltage of 180 kV. However, the

Table 2

Results obtained for mechanical properties of samples.

Sample	Compressive strength (MPa)	Flexural strength (MPa)	Elastic modulus (GPa)
30_00	76.6 ± 1.4	5.5 ± 0.3	42.8 ± 2.5
30_05	75.1 ± 2.9	5.3 ± 0.2	43.6*
30_10	77.3 ± 1.8	4.9 ± 0.3	42.9 ± 1.6
40_00	50.8 ± 5.8	3.9 ± 0.3	35.2 ± 0.8
40_05	46.0 ± 1.0	4.5 ± 0.3	39.1*
40_10	49.2 ± 1.7	4.1 ± 0.2	34.6 ± 0.8
50_00	44.9 ± 1.1	3.7 ± 0.2	30.7 ± 0.7
50_05	43.1 ± 0.2	3.6 ± 0.3	30.0*
50_10	41.3 ± 1.9	3.4 ± 0.2	28.4 ± 1.4

* Value estimated using Eq. 2

Table 3

Results obtained for air content, connectivity and tortuosity of the pore space of the samples.

Sample	Air content (%)	MIP connectivity (%)	Tomography tortuosity
30_00	4.8	24.96	1.03
30_05	4.3	25.26	1.82
30_10	4.1	32.97	3.27
40_00	3.0	38.55	1.02
40_05	3.4	36.80	1.32
40_10	4.6	38.49	1.33
50_00	0.8	48.52	1.09
50_05	1.8	45.75	1.38
50_10	2.2	47.87	1.62

acquisitions were performed at 100 kV. Samples were placed at a distance of 25.99 mm from the transmission tube and 199.99 mm from the detector. A magnification of

7.69 was acquired, achieving a 6.49 μm voxel size. Reconstruction of the CT images was done through Datos VeloCT. Additionally, a median filter was applied through VGStudio Max 3.0.

The reconstructed CT images were processed using the Freeware Fiji image analysis [56]. In total 1520 images from the middle of each sample were chosen for the image stacks, which equals to a 9.87 mm sample height. Through the plugin Trainable Weka Segmentation [57], a binary stack is created containing only the pores and fibres. Subsequently, this binary stack was used in the pore analysis. A second plugin (BoneJ [58]) was used to determine the geometric properties of each individual pore detected. The data set was further treated by Matlab [59] to obtain the pore size distribution of each mixture.

Pore connectivity was analysed through a tortuosity plugin [60] in ImageJ [61]. Assuming material tortuosity is inversely related to pore connectivity, a property value is acquired for the pore connectivity of large pores of the samples. The tortuosity was analyzed for each data set in the five directions of heating (because the cylinders for spalling experiments rest on top of a refractory bed inside the oven, each sample is heated only on the sides and top, not on the bottom).

3. Results

3.1. Fundamental samples properties

Table 2 contains the results for the mechanical properties of the samples. As expected, strength and elastic modulus decrease with increasing W/C ratio.

Table 3 contains the results for the porosity of the samples. Although techniques such as MIP and μCT provide large data sets regarding the pore structure, this paper focuses on the parameters used for the prediction of spalling behavior. Given the increasing fluidity of the fresh mixtures with increasing W/C ratio, air content decreases proportionally. Meanwhile, connectivity of capillary pores, as determined by Eq. 3, increases with W/C ratio. However, the connectivity of macro-pores, as

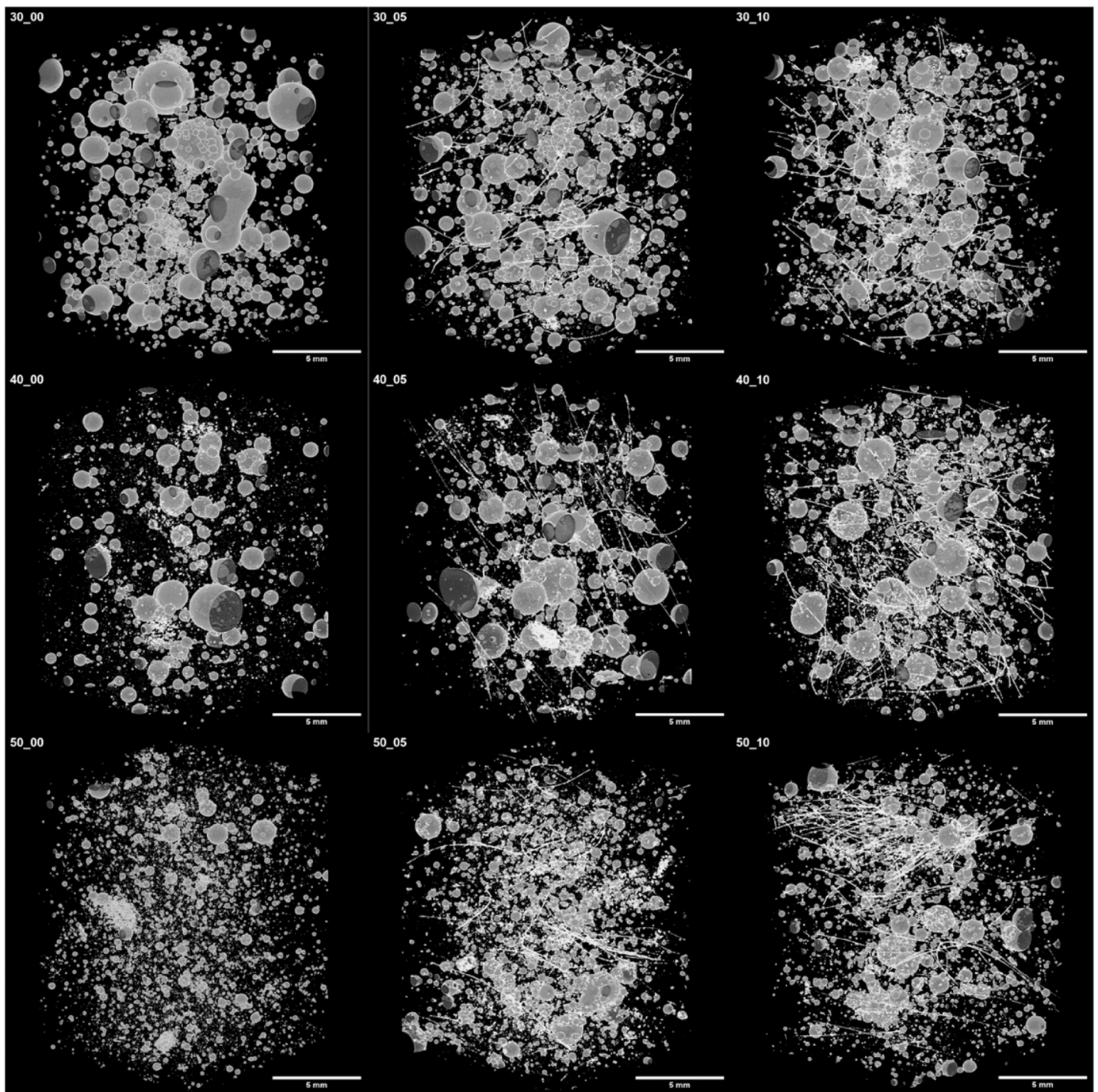


Fig. 2. X-ray microtomography representation of macro pore volumes for each mixture.

determined by computer tomography, appears to be relatively insensitive to W/C ratio variation, it increases proportionally to polypropylene fibres content.

Fig. 2 contains a three-dimensional representation of the macroporosity and fibres of the samples as detected by μ CT. The PP fibres can be observed as thin white filaments. An increase in macro-pores is observed with both, the increases in fiber content, and the decrease of W/C ratio, in accordance with the air content tests. Fig. 3

3.2. Spalling behaviour

compiles the results of the heating experiment. Although not all samples parameter combinations could be tested, other works [62–65]

already determined that samples with same size and mixture composition may spall with increasing heating rates. As follows, if a mixture did not spall at 50 °C/min, it should not spall at a lower heating rate. Accordingly, if a mixture spalls at 10 °C/min, stands to logic that it would spall at a higher heating rate.

All mixtures without polypropylene fibres suffered from spalling, regardless of heating rate or W/C ratio. Mixtures with 0.10% of PP content did not suffer from spalling regardless of the W/C ratio or heating rate. The mixtures with 0.05% PP content did not spall for 0.30 W/C ratio, but did spall for 0.40 and 0.50 ratios when the heating rate was increased from 10 °C/min to 30 °C/min (and follow the trend at 50 °C/min). This disparity might seem counter intuitive since the

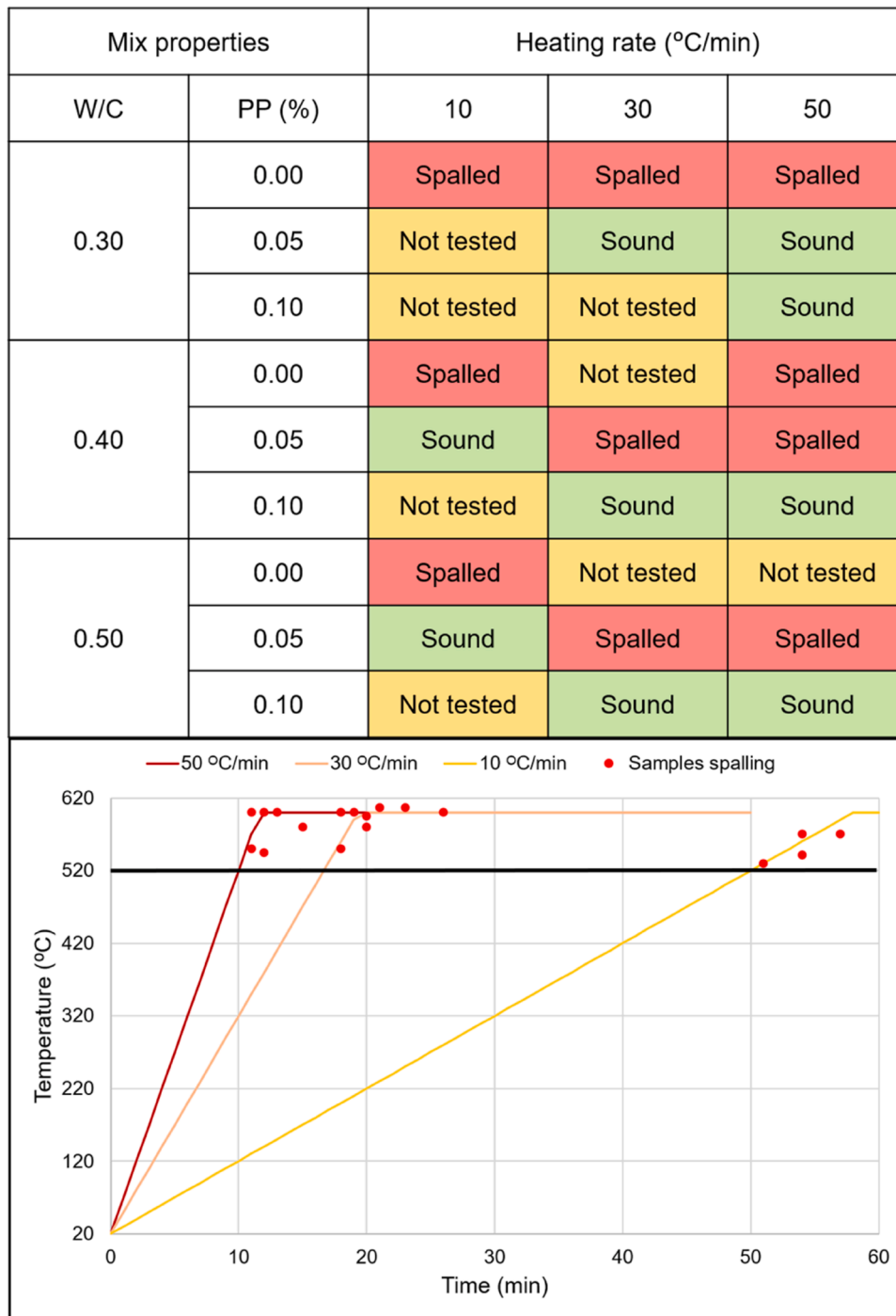


Fig. 3. Spalling testing results. Top: Different mixtures reaction to oven heating at 10, 30 and 50 °C/min. Bottom: Moment and temperature of spalling for each tested sample.

samples with lower W/C ratio performed better, however, the actual determining factor to reduce the resistance against

spalling is the concrete denser microstructure, rather than just the amount of mixture water [11–13]. In the present experiment, the low viscosity of the mixtures generated a considerably higher amount of entrapped air in the samples with W/C ratio = 0.30, as it can be observed on Table 3 and Figure

2. These are valuable data points as it indicates a higher influence of macro-porosity than micro-porosity for spalling resistance. Which is reinforced by the MIP connectivity results, which were not affected by the material fresh state consistency and increased proportionally to the

W/C ratio. In addition,

all samples spalled within 10 minutes of surpassing 500°C, despite different

heating rates. This might be an indication of the volume to heated area ratio

influence in this heating regime.

Further, the samples displayed different degrees of spalling, depending on the amount of fibres and heating ratio. Fig. 4 shows some examples of samples after the heating experiment. It seems the W/C ratio did not influence the size of pieces as much as the other parameters.

	HR = 10°C/min	HR = 30°C/min	HR = 50°C/min
PP = 0.00%	<p>Big pieces</p>  <p>30_00_10/SCI = 0.19</p>  <p>50_00_10/SCI = 0.14</p>	<p>Small pieces</p>  <p>30_00_30/SCI = 0.11</p>	<p>Small pieces</p>  <p>30_00_50/SCI = 0.09</p>  <p>40_00_50/SCI = 0.04</p>
PP = 0.05%	<p>No spall</p>  <p>40_05_10 SCI = 1.73</p> <p>50_05_10 SCI = 1.30</p>	<p>Big pieces</p>  <p>40_05_30/SCI = 0.99</p>  <p>50_05_30/SCI = 0.75</p>	<p>Small pieces</p>  <p>40_05_50/SCI = 0.77</p>  <p>50_05_50/SCI = 0.58</p>

Fig. 4. Examples of spalling intensity in selected samples (SCI is a measure explained in the Equation development section).

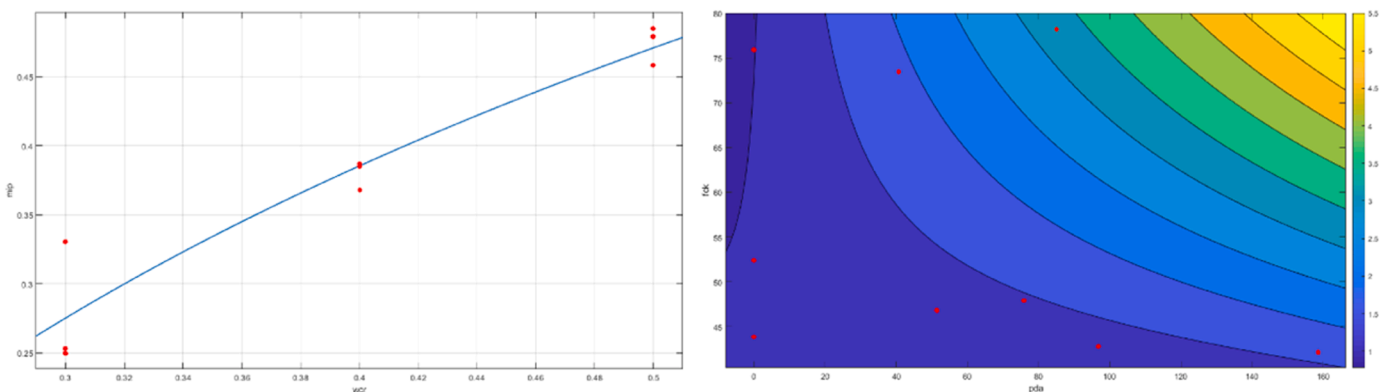


Fig. 5. Regression of $\Lambda_{(MP)}$ using the experimental results of Section 3 and Eq. 9 (left); and $\Lambda_{(\mu_{CT})}$ using the same results and Eq. 10 (right).

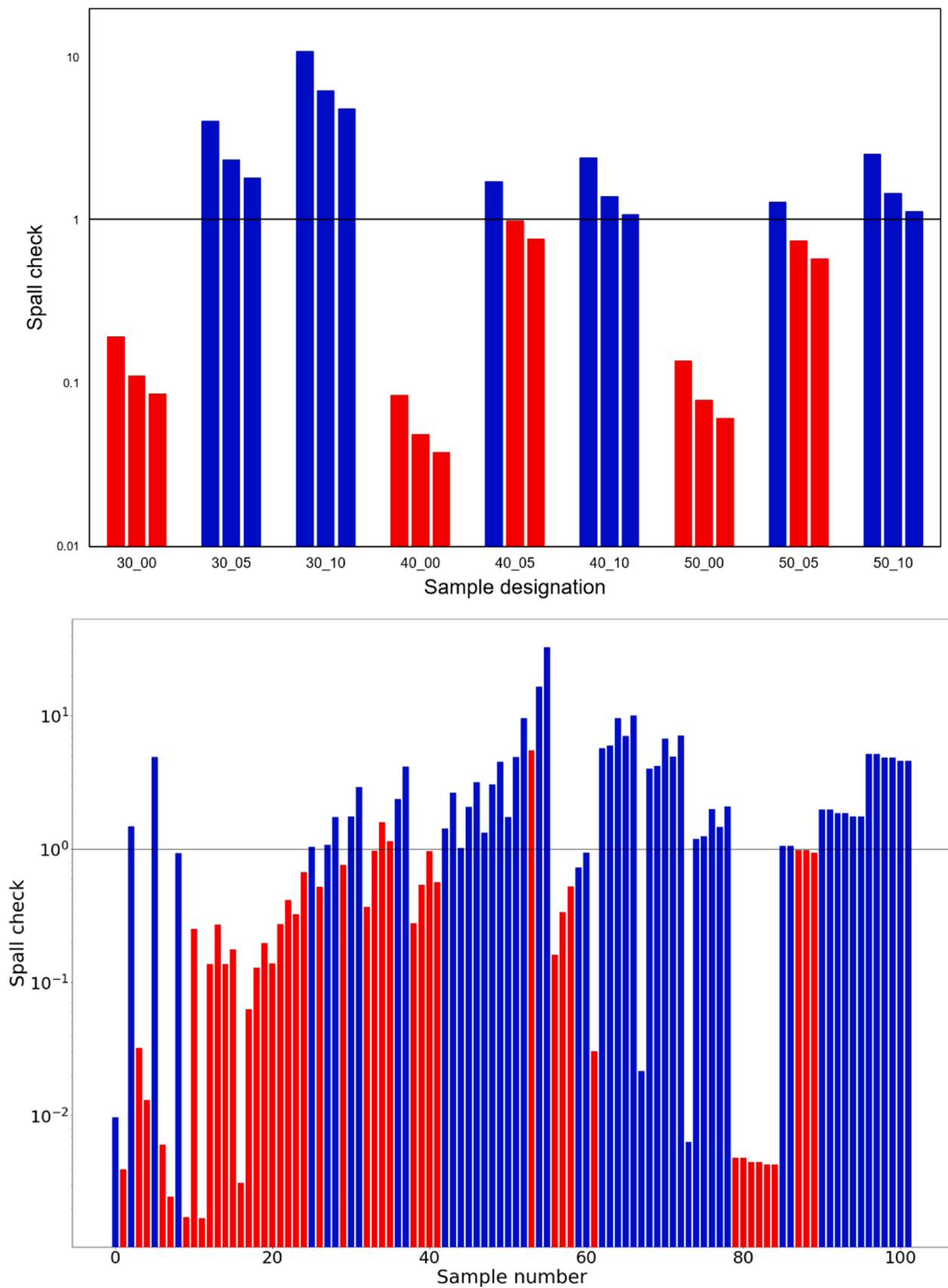


Fig. 6. Validation of Eq. 5 using spalling experiments. Blue lines represent samples that did not spall, red lines represent samples that did spall, the black horizontal lines shows the prediction cutoff for spalling. Top: Results from experiment described in the present paper, each mix design has three lines to represent the tests performed at 10 °C/min, 30 °C/min and 50 °C/min, in this order. Bottom: Results from experiments collected from the selected papers [63,80–83], samples are organized in no particular order.

4. Equation development

4.1. Assumptions

As previously stated, spalling usually occurs in concrete as a combination of thermo-mechanical spalling and hydro-thermal spalling. For this work, it was assumed Eq. 1 could describe a theoretical concrete material without porosity. Although such material is impossible to be achieved, this represents a starting point for the adaptation of the work of Lu & Fleck (1998) [29] for cementitious materials. Re-writing Eq. 1 to separate the variables based on physical meaning, it yields Eq. 4, in which the first term describes the contribution of the mechanical properties of the material to the resistance against thermal shock cracking, the second term describes the influence of the environment and the third term describes the contribution of the thermal properties, sample size and geometry. Fig. 5

$$\Delta T = \frac{\sigma_t}{E} \cdot \frac{C_2}{h} \cdot \frac{k}{\alpha \cdot H} \quad (4)$$

While W/C ratio is of relatively low influence for the third term [66] and no impact on the second term, it controls the values of the first term of Eq. 4. However, the effect of varying W/C ratio within the studied ranges seem to be negligible for the ratio between tensile strength and elastic modulus of the material. This seems intuitively wrong, since several

experiments show that changing W/C ratio in cementitious materials can significantly alter the spalling resistance [24,66,67]. Presently, it is accepted that this is mostly caused by the lower permeability and increased brittleness of the paste [68,69]. Both these properties are correlated to changes in capillary porosity [70,71], which increases proportionally to the W/C ratio [72]. While brittleness addressed through the elastic modulus, changes in permeability caused by decrease of W/C ratio are unaccounted for. However, Table 2 in Section 3 shows that MIP connectivity seems proportional to changes in W/C ratio. Thus, the authors propose a variable $\Lambda_{(MIP)}$ that represents the connectivity of micro-pores based on Eq. 3 to be added to the first term of Eq. 4. This addition is placed on the numerator, as the increase in capillary connectivity should improve concrete resistance to spalling [55,73].

As the main feature of the THM, instead of attempting to estimate pore pressure at several scales, the authors include the capacity of the material to allow vapour to escape. The vapour pressure is proportional to the thermal gradient and water mass within the sample [74]. The thermal gradient is dependent of sample size, geometry, thermal conductivity and heating rate. The sample size and geometry are already described by the variable H , as well as thermal conductivity by the variable k . Because Eq. 1 was developed for immediate thermal shock events, heating rate still needs to be added. Using the available data set, it seems that the heating rate (HR) is inversely proportional to the square of the sample resistance to spalling. Thus, it is added in the denominator as the square root of heating rate.

The free water mass in the material can be approximated using the amount of macro-porosity and saturation level of the concrete. The authors included the variable AC as the air content and φ_s as the saturation degree. For a mix with same permeability, increasing saturation degree seems to make spalling much more likely [75], as intuitively inferred by the higher amount of water vapor in need to escape, thus φ_s is placed on the denominator of the equation. On the other hand, AC is placed on the numerator, despite possibly allowing for more water to be held within the material. This is because this properties has been found to not affect the tensile strength and elastic modulus of concrete under spalling temperatures, but allow for comparatively higher escape of water [76], thus improving the material resistance to spalling.

Finally, the actual capacity of macro-porosity to allow vapor transport must be related to its connectivity in addition to its volume. This is reflected

in Figs. 3 and 4 that highlight the PP fibre content as a key parameter

for spalling prediction. As described in Section 2, the tortuosity of the paste can be used as connectivity for the macro-pore space and is introduced as $\Lambda_{(\mu CT)}$. The authors defend the use of this tortuosity parameter in opposition to fibre content because, although indirect, $\Lambda_{(\mu CT)}$ is a physical measure of the connections between the macro-pores in a given sample. Meanwhile, fibre content does not take into account the influence of fibre diameter, length and aggregate size and content, all of which influence spalling behaviour [77,78]. As this is one of the main forms of spalling prevention, the parameter is placed on the numerator. Because tortuosity is measured in small volumes and upscaling remains a challenge [79], the authors considered the relationship with sample volume (and geometry) non-linear and added a constant C_3 to account for that. This resulted in Eq. 5:

$$SCI = \frac{\sigma_t \cdot (\Lambda_{(MIP)} - C_1)}{E} \cdot \frac{C_2}{h} \cdot \frac{k \cdot AC}{\alpha \cdot \sqrt{HR}} \cdot \frac{\Lambda_{(\mu CT)} - 1}{H^{C_3} \cdot \varphi_s} \quad (5)$$

In which $C_1 = 0.02$, $C_2 = 180$, $C_3 = 0.17$ and the left hand side of the equation no longer means a critical thermal gradient, but a spalling control index (SCI). The constants were set so a value of $SCI < 1$ denotes spalling and $SCI > 1$ predicts that the studied concrete will not spall under the considered conditions. The value of the constants has been calibrated using the experiment described in the present paper.

4.2. Validation

Although Eq. 5 correctly predicts whether the studied samples would spall or not (Fig. 6, top), the amount of data was not enough to be considered statistically significant. For this reason, five studies [63, 80–83] were selected for the validation of the proposed equation. The main criteria to chose relevant research papers were the publication of heating experiments in which the following parameters were reported: if the samples spalled, the W/C ratio, the volume, the heated area, the polypropylene fibres content and dimensions (if used), the compressive strength, the air content and the heating rate. Since the experiment in the present paper used saturated samples, the search was limited to experiments also using saturated samples.

Ideally, tensile strength and elastic modulus would be part of the searching criteria, however, these values are rarely published after spalling experiments. To circumvent this challenge, the authors estimated tensile strength and elastic moduli for samples lacking these data based on the Eurocode [84].

Within the norm, it is stated that the tensile strength of concretes of class C50/60 or below can be estimated based on Eq. 6, while concretes above this class use Eq. 7. The elastic moduli were estimated using Eq. 8. Further, these would be the values for the material at room temperature, it would not be feasible to gather enough literature results including mechanical properties at high temperatures. In a review performed by Ma et al. (2015) [23], it was estimated that about 25% of the flexural strength and elastic modulus of concrete is lost at a temperature of 250°C,

thus, a 0.75 factor was applied to the estimation of these properties.

$$f_{cm} = 0.3 \cdot f_{ck}^{2/3} \quad (6)$$

$$f_{cm} = 2.12 \cdot \ln \left(1 + \left(\frac{f_{cm}}{10} \right) \right) \quad (7)$$

$$E_{cm} = 22 \cdot \left(\frac{f_{cm}}{10} \right)^{0.3} \quad (8)$$

In which f_{cm} is the mean tensile strength of the sample, f_{ck} is the design compressive strength, f_{cm} is the mean compressive strength and E_{cm} is the mean Young's modulus as described on the Eurocode [84].

The heat transfer coefficient between concrete and air was assumed to be 10 W/m²/K, the thermal conductivity of the samples was set at 1.8 W/m/K, and the coefficient of thermal dilation as 4.5·10⁻⁵ 1/K [85].

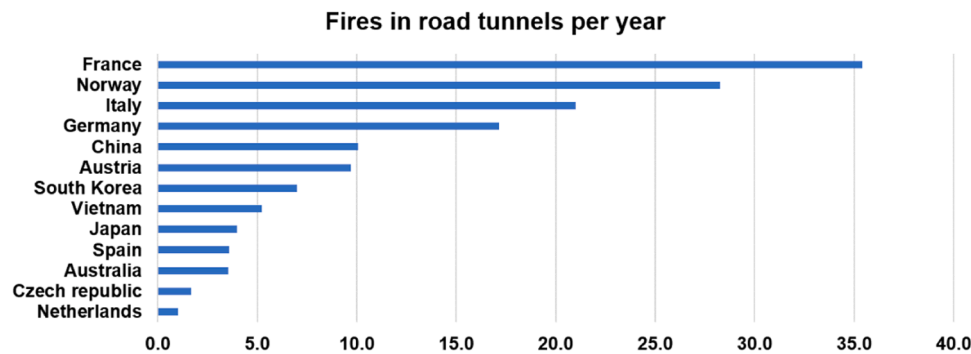


Fig. 7. Average occurrence of fires in road tunnels for different countries, data extracted from [95,98,99].

Since $\Lambda_{(MIP)}$ and $\Lambda_{(\mu CT)}$ were newly proposed parameters, these had to be estimated for all literature samples. For both parameters, regressions were performed using the experiment described in Section 3. As expected, $\Lambda_{(MIP)}$ is proportional to W/C ratio, with a logarithmic relation in the shape of Eq. 9, which yields a $R^2 = 0.9222$. For the paste tortuosity, a second order polynomial regression with two variables was used based on the fibre properties, air content and compression strength, generating Eq. 10 with a $R^2 = 0.9911$. shows the fitting and data scatter for the two regressions.

$$\Lambda_{(MIP)} = 0.3829 \cdot \ln(W/C \text{ ratio}) + 0.7362 \quad (9)$$

$$\Lambda_{(\mu CT)} = 1.194 - 3.034e^{-2} \cdot P_{adj} - 2.675e^{-3} \cdot f_{ck} + 2.837e^{-5} \cdot P_{adj}^2 + 6.955e^{-4} \cdot P_{adj} \cdot f_{ck} \quad (10)$$

In which the P_{adj} is the polypropylene index divided by the air content of the sample. The concept of PP index was first proposed by Li et al. (2021) [44], as a better description of the amount and spacing of PP fibres inside concrete. This index is defined as the fiber dosage times fiber length divided by its diameter.

The five selected papers [63,80–83] contain a total of 102 unique samples that went through heating experiments. These samples varied in volume from 9 dm³ to 216 dm³, in air content from 1.6% to 4.2%, in heating rate from 5 °C/min to 115 °C/min and in PP index from 0 to 4700. Eq. 5 was used to predict the behaviour of each individual sample, with the results reported in Fig. 6, bottom.

A total of 93 correct predictions was achieved, which is equivalent to 91.18% accuracy. As shown in Fig. 6, from the 9 incorrect predictions, only 3 belong to samples that did spall when Eq. 5 indicated a safe situation. The remaining 6 incorrect data points belong to sound samples that were expected to spall.

5. Discussion

Although Eq. 5 reached high accuracy when compared against other laboratory experiments, further work is necessary to predict spalling in actual concrete structures. During fires, the material often experiences one-sided heating, which allows for bigger temperature gradients with faster development. Some works have been published in the shortcomings of sample size and oven heating regarding the study of concrete in high temperatures [83,86–89], however, this remains as the most accessible option and vast majority of published research. In order to take more realistic setups in consideration (e. g. a full size reinforced concrete beam under fire), a much broader experimental campaign would be necessary. However, it is often better to first study the influence of individual variable in detail prior to conduct large-scale tests, which is what was attempted in this work.

Another drawback is that concrete in a structure is never fully saturated, it always possess an inner gradient. This causes a small amount of stress in the structure by default, prior to any thermal loading. Some researchers [75,90] looked into the influence of different

saturation degrees in concrete regarding spalling, but these samples were treated to have a constant saturation through its entirety. The actual gradient found in structures is not only related to the material properties, as it is also linked to the structure design and in which area is the concrete located.

Further, samples were free to expand at the surfaces inside the oven, while most concrete structures are externally restrained and under loads, which changes the response to high temperatures [91]. Although several works attempted to study this issue [34,92,93], these do not account for relaxation of stress. In actual structures, relaxation develops over years of sustained load and increases with temperature [94]. This effect will lessen the stresses caused by the restraining of the material within the structure and should be accounted for.

Still, development in the field of spalling prediction is necessary to achieve prevention. This is a phenomenon that poses great danger for structures with difficult evacuation in the case of fires. Tunnels, for example, can be greatly affected by it, which is not a rare occurrence [95], indeed, most incidents involving trains in tunnels are fire related [96]. Fig. 7 shows the average amount of fires (caused by automobiles, trucks or trains) to occur inside tunnels in different countries. While the priority is to avoid loss of life, these events also cause great damage to the concrete lining, demanding costly repairs that hinder traffic [21,97]. Thus, spalling-proof concrete mixture must be developed and used in these structures.

6. Conclusions

Although high temperature spalling is a known problem in concrete for nearly a century, the prediction of structural members behaviour against rapid heating is still a challenge. Most standards merely advice a minimum polypropylene fiber content to protect structures from it. However, spalling may affect structures even with high amounts of fibres, depending on physical and geometrical properties of the fiber itself [21,100].

While computational methods are very useful for the advancement of spalling prediction, these are often insensitive to mixture variations or fiber properties within concrete [37–40], which hinders their broader application by practice engineers. Some most recent numerical approaches (such as Ren et al. (2021) [101]) have a very encompassing solution for the estimation of spalling. However, the goals of this paper was to develop a somewhat simpler approach that would be accessible to a wider audience of engineers looking for solutions against spalling in specific applications.

To this end, the paper proposes an analytical equation that determines whether a given concrete sample will suffer spalling under fast heating conditions. To achieve this, a preliminary experimental campaign was executed in order to obtain measures of connectivity within the pore space. The authors make a distinction between capillary porosity and macro pores, as the connectivity of each of these systems may differ considerably for variations in mixture parameters such as W/

C ratio, use of PP fibres or air entertainment. The equation was then validated using over 100 examples from literature. With an accuracy higher than 91.2%, this seems a viable alternative for spalling prediction of laboratory concrete.

However, spalling does not depend only on the material, but of a combination of material and structural parameters. This has been partially argued in the Discussion section and offers insight on future work. Although functional, Eq. 5 could be complemented by a research on the influence of saturation gradients within concrete and loaded, reinforced samples.

Declaration of Competing Interest

The authors declare that they have no known competing financial interests or personal relationships that could have appeared to influence the work reported in this paper.

Data availability

Data will be made available on request.

Acknowledgements

The authors would like to thank Tata Steel IJmuiden B.V. for the financial support.

References

- Ahrens, M., & Maheshwari, R. (2020). Home Structure Fires. NFPA technical report. Retrieved from: <https://www.nfpa.org/News-and-Research/Data-research-and-tools/Building-and-Life-Safety/Home-Structure-Fires> on 2nd of September, 2021.
- Eurocode (2002) NEN-EN 1991-1-2:2002. Eurocode 1: Actions on structures - Part 1-2: General actions - Actions on structures exposed to fire. Brussels, European committee for standardization.
- Neville, A.M. (2011). Properties of Concrete. Essex: Pearson Education Limited. ISBN:9780273755807.
- Mehta, P.K., & Monteiro, P.J.M. (2006). Concrete: Microstructure, Properties, and Materials. Berkeley: McGraw-Hill Education. ISBN:9780071462891.
- Bertolini, L. (2010). Materiais de Construção (in Portuguese). São Paulo: Oficina de textos. ISBN:9788579750106.
- Han, B., & Zhang, L. (2017). Smart and Multifunctional Concrete Toward Sustainable Infrastructures. Singapore: Springer. ISBN:9789811043482.
- H. sheng Shi, B. wan Xu, X. chen Zhou, Influence of mineral admixtures on compressive strength, gas permeability and carbonation of high performance concrete, *Constr. Build. Mater.* 23 (5) (2009) 1980–1985, <https://doi.org/10.1016/j.conbuildmat.2008.08.021>.
- M.R. Geiker, P. Laugesen, On the effect of laboratory conditioning and freeze/thaw exposure on moisture profiles in HPC, *Cem. Concr. Res.* 31 (12) (2001) 1831–1836, [https://doi.org/10.1016/S0008-8846\(01\)00643-3](https://doi.org/10.1016/S0008-8846(01)00643-3).
- X. Quan, S. Wang, K. Liu, N. Zhao, J. Xu, F. Xu, J. Zhou, The corrosion resistance of engineered cementitious composite (ECC) containing high-volume fly ash and low-volume bentonite against the combined action of sulfate attack and dry-wet cycles, *Constr. Build. Mater.* 303 (August) (2021) 124599, <https://doi.org/10.1016/j.conbuildmat.2021.124599>.
- B.A. Gedam, Time-dependent behaviour prediction of the prestressed HPC I-girder, *Eng. Struct.* 201 (October) (2019) 109763, <https://doi.org/10.1016/j.engstruct.2019.109763>.
- Pimenta, P., Mindeguia, J.C., Simon, A., & Behloul, M. (2011). Behaviour of UHPFRC at High Temperatures. In: Toutlemonde, F., & Resplendino, J. Designing and Building with UHPFRC. London: Wiley. ISBN:9781848212718.
- Bei, S., & Zhixiang, L. (2016). Investigation on spalling resistance of ultra-high-strength concrete under rapid heating and rapid cooling. *Case Studies in Construction Materials*, 4, 146–153. <https://doi.org/10.1016/j.cscm.2016.04.001>.
- G. Peng, X. Niu, Y. Shang, D. Zhang, X. Chen, H. Ding, Combined curing as a novel approach to improve resistance of ultra-high performance concrete to explosive spalling under high temperature and its mechanical properties. *Cem. Concr. Res.* 109 (March) (2018) 147–158, <https://doi.org/10.1016/j.cemconres.2018.04.011>.
- M.Z. Naser, Heuristic machine cognition to predict fire-induced spalling and fire resistance of concrete structures, *Autom. Constr.* 106 (2019) 102916, <https://doi.org/10.1016/j.autcon.2019.102916>.
- V.N. Aptukov, Model of thermoviscoelastoplastic material damage application to spalling failure, *Fiz. Goreniya i Vzryv* 22 (2) (1986) 244–253.
- K.D. Hertz, Limits of spalling of fire-exposed concrete, *Fire Saf. J.* 38 (2003) 103–116.
- Y.W.Y.F.C. Poon, C. Tang, Spalling of concrete cover of fiber-reinforced polymer reinforced concrete under thermal loads, *Mater. Struct.* (2006) 991–999, <https://doi.org/10.1617/s11527-005-9032-5>.
- K. Mróz, I. Hager, K. Korniejenko, Material solutions for passive fire protection of buildings and structures and their performances testing, *Procedia Eng.* 151 (2016) 284–291, <https://doi.org/10.1016/j.proeng.2016.07.388>.
- F. Wang, M. Wang, J. Huo, The effects of the passive fire protection layer on the behavior of concrete tunnel linings: a field fire testing study, *Tunn. Undergr. Space Technol.* 69 (June) (2017) 162–170, <https://doi.org/10.1016/j.tust.2017.06.021>.
- M. Lahoti, K. Hai, E. Yang, A critical review of geopolymer properties for structural fire-resistance applications, *Constr. Build. Mater.* 221 (2019) 514–526, <https://doi.org/10.1016/j.conbuildmat.2019.06.076>.
- C. Maluk, J. Tignard, A. Ridout, T. Clarke, R. Winterberg, Experimental study on the fire behaviour of fibre reinforced concrete used in tunnel applications, *Fire Saf. J.* 120 (January) (2021) 103173, <https://doi.org/10.1016/j.firesaf.2020.103173>.
- J. Duan, Y. Dong, J. Xiao, D. Zhang, W. Zheng, S. Zhang, A large-scale fire test of an immersed tunnel under the protection of fire resistive coating, *Tunn. Undergr. Space Technol.* 111 (7) (2021) 103844, <https://doi.org/10.1016/j.tust.2021.103844>.
- Q. Ma, R. Guo, Z. Zhao, Z. Lin, K. He, Mechanical properties of concrete at high temperature — a review, *Constr. Build. Mater.* 93 (2015) 371–383, <https://doi.org/10.1016/j.conbuildmat.2015.05.131>.
- M. Abid, X. Hou, W. Zheng, R. Rizwan, High temperature and residual properties of reactive powder concrete – a review, *Constr. Build. Mater.* 147 (519) (2017) 339–351, <https://doi.org/10.1016/j.conbuildmat.2017.04.083>.
- F.W. Preston, H.E. White, Observations on spalling, *J. Am. Ceram. Soc.* 17 (1–12) (1934) 137–144, <https://doi.org/10.1111/j.1151-2916.1934.tb19296.x>.
- Bazant, Z. (1997). Analysis of Pore Pressure, Thermal Stress and Fracture in Rapidly Heated Concrete. International Workshop on Fire Performance of High-Strength Concrete. Proceedings. Appendix B: Workshop Papers. B10, Gaithersburg, MD, [online], https://tsapps.nist.gov/publication/get_pdf.cfm?pubid=916655 (Accessed August 31, 2022).
- J. Yang, G.F. Peng, J. Zhao, G.S. Shui, On the explosive spalling behavior of ultra-high performance concrete with and without coarse aggregate exposed to high temperature, *Constr. Build. Mater.* 226 (2019) 932–944, <https://doi.org/10.1016/j.conbuildmat.2019.07.299>.
- Rishel, D.M., Pettit, F.S., Birks, N. (1993). Spalling types and mechanisms in the erosion corrosion of metals at high temperature. *Corrosion Science*, 35, 5–8, pp. 1007–1013. [https://doi.org/10.1016/0010-938X\(93\)90319-C](https://doi.org/10.1016/0010-938X(93)90319-C).
- Lu, T.J., Fleck, N.A. (1998). The Thermal Shock Resistance of Solids. *Acta Materialia*, 46(13), 4755–4768. [https://doi.org/10.1016/S1359-6454\(98\)00127-X](https://doi.org/10.1016/S1359-6454(98)00127-X).
- Y. Zhang, M. Zeiml, M. Maier, Y. Yuan, R. Lackner, Fast assessing spalling risk of tunnel linings under RABT fire: from a coupled thermo-hydro-chemo-mechanical model towards an estimation method, *Eng. Struct.* 142 (2017) 1–19, <https://doi.org/10.1016/j.engstruct.2017.03.068>.
- J.C. Liu, Y. Zhang, A simplified model to predict thermo-hygral behaviour and explosive spalling of concrete, *J. Adv. Concr. Technol.* 17 (7) (2019) 419–433, <https://doi.org/10.3151/jact.17.419>.
- F. Lo Monte, R. Felicetti, A. Meda, A. Bortolussi, Assessment of concrete sensitivity to fire spalling: a multi-scale experimental approach, *Constr. Build. Mater.* 212 (2019) 476–485, <https://doi.org/10.1016/j.conbuildmat.2019.03.332>.
- P. Kalifa, F.D. Menneveau, D. Quenard, Spalling and pore pressure in HPC at high temperatures, *Cem. Concr. Res.* 30 (12) (2000) 1915–1927, [https://doi.org/10.1016/S0008-8846\(00\)00384-7](https://doi.org/10.1016/S0008-8846(00)00384-7).
- F.A. Ali, D. O'Connor, A. Abu-Tair, Explosive spalling of high-strength concrete columns in fire, *Mag. Concr. Res.* 53 (3) (2001) 197–204, <https://doi.org/10.1680/macrc.2001.53.3.197>.
- M. Zeiml, D. Leithner, R. Lackner, H. Mang, How do polypropylene fibres improve the spalling behavior of in-situ concrete? *Cem. Concr. Res.* 36 (2006) 929–942, <https://doi.org/10.1016/j.cemconres.2005.12.018>.
- X. Liu, G. Ye, G. De Schutter, Y. Yuan, L. Taerwe, On the mechanism of polypropylene fibres in preventing fire spalling in self-compacting and high-performance cement paste, *Cem. Concr. Res.* 38 (4) (2008) 487–499, <https://doi.org/10.1016/j.cemconres.2007.11.010>.
- Y. Zhang, M. Zeiml, C. Pichler, R. Lackner, Model-based risk assessment of concrete spalling in tunnel linings under fire loading, *Eng. Struct.* 77 (2014) 207–215, <https://doi.org/10.1016/j.engstruct.2014.02.033>.
- M. Beneš, R. SStefan, Hygro-thermo-mechanical analysis of spalling in concrete walls at high temperatures as a moving boundary problem, *Int. J. Heat. Mass Transf.* 85 (2015) 110–134, <https://doi.org/10.1016/j.jheatmasstransfer.2015.01.050>.
- Y. Zhang, M. Zeiml, M. Maier, Y. Yuan, R. Lackner, Fast assessing spalling risk of tunnel linings under RABT fire: from a coupled thermo-hydro-chemo-mechanical model towards an estimation method, *Eng. Struct.* 142 (2017) 1–19, <https://doi.org/10.1016/j.engstruct.2017.03.068>.
- A. Caggiano, D.S. Schicchi, G. Etse, M. Ripani, Meso-scale response of concrete under high temperature based on coupled thermo-mechanical and pore-pressure interface modeling, *Eng. Fail. Anal.* 85 (November 2017) (2018) 167–188, <https://doi.org/10.1016/j.engfailanal.2017.11.016>.
- D. Gawin, F. Pesavento, B.A. Schrefler, Towards prediction of the thermal spalling risk through a multi-phase porous media model of concrete, *Comput. Methods*

- Appl. Mech. Eng. 195 (41) (2006) 5707–5729, <https://doi.org/10.1016/j.cma.2005.10.021>.
- [42] P. Cheng, H. Zhu, Z. Yan, Y. Shen, J. Fish, Multiscale modeling for fire induced spalling in concrete tunnel linings based on the superposition-based phase field fracture model, *Comput. Geotech.* 148 (2022) 104832, <https://doi.org/10.1016/j.compgeo.2022.104832>.
- [43] F. Lo Monte, R. Felicetti, M.J. Miah, The influence of pore pressure on fracture behaviour of Normal-Strength and High-Performance Concretes at high temperature, *Cem. Concr. Compos.* 104 (2019) 103388, <https://doi.org/10.1016/j.cemconcomp.2019.103388>.
- [44] Y. Li, E. Yang, A. Zhou, T. Liu, Pore pressure build-up and explosive spalling in concrete at elevated temperature: a review, *Constr. Build. Mater.* 284 (2021) 122818, <https://doi.org/10.1016/j.conbuildmat.2021.122818>.
- [45] G.R. Consolazio, M.C. McVay, J.W. Rish, Measurement and prediction of pore pressures in saturated cement mortar subjected to radiant heating, *Acids Mater. J.* 95 (5) (1998) 525–536, <https://doi.org/10.14359/395>.
- [46] P. Kalifa, G. Chené, C. Galle, High-temperature behaviour of HPC with polypropylene fibres, *Cem. Concr. Res.* 31 (10) (2001) 1487–1499, [https://doi.org/10.1016/S0008-8846\(01\)00596-8](https://doi.org/10.1016/S0008-8846(01)00596-8).
- [47] L.T. Phan, Pore pressure and explosive spalling in concrete, *Mater. Struct.* 41 (2008) 1623–1632, <https://doi.org/10.1617/s11527-008-9353-2>.
- [48] Mindeguia, J., Carré, H., Pimienta, P., & Borderie, C.La (2015). Experimental discussion on the mechanisms behind the fire spalling of concrete. *Fire and Materials*, June 2014, 619–635. <https://doi.org/10.1002/fam>.
- [49] NEN-EN 196-1:2016; Methods of testing cement – Part 1: Determination of strength. *Nederlands Normalisatie-Instituut*: Delft, The Netherlands, 2016.
- [50] NEN-EN 12390-3:2019; Testing hardened concrete – Part 3: Compressive strength of test specimens. *Nederlands Normalisatie-Instituut*: Delft, The Netherlands, 2019.
- [51] NEN-EN 12390-5:2019; Testing hardened concrete – Part 5: Flexural strength of test specimens. *Nederlands Normalisatie-Instituut*: Delft, The Netherlands, 2019.
- [52] NEN-EN 12390-3:2021; Testing hardened concrete – Part 13: Determination of secant modulus of elasticity in compression. *Nederlands Normalisatie-Instituut*: Delft, The Netherlands, 2021.
- [53] NEN-EN 1015-7:1998; Methods of test for mortar for masonry – Part 7: Determination of air content of fresh mortar. *Nederlands Normalisatie-Instituut*: Delft, The Netherlands, 1998.
- [54] J. Zhang, G.W. Scherer, Comparison of methods for arresting hydration of cement, *Cem. Concr. Res.* 41 (10) (2011) 1024–1036, <https://doi.org/10.1016/j.cemconres.2011.06.003>.
- [55] Z. Yu, C. Ni, M. Tang, X. Shen, Relationship between water permeability and pore structure of Portland cement paste blended with fly ash, *Constr. Build. Mater.* 175 (2018) 458–466, <https://doi.org/10.1016/j.conbuildmat.2018.04.147>.
- [56] J. Schindelin, I. Arganda-Carreras, E. Frise, V. Kaynig, M. Longair, T. Pietzsch, S. Preibisch, C. Rueden, S. Saalfeld, B. Schmid, J. Tinevez, D. White, V. Hartenstein, K. Eliceiri, P. Tomancak, A. Cardona, Fiji: an open-source platform for biological-image analysis, *Nat. Methods* 9 (2012) 676–682, <https://doi.org/10.1038/nmeth.2019>.
- [57] I. Arganda-Carreras, V. Kaynig, C. Rueden, K.W. Eliceiri, J. Schindelin, A. Cardona, H. Sebastian Seung, Trainable Weka Segmentation: a machine learning tool for microscopy pixel classification, *Bioinformatics* 33 (15) (2017) 2424–2426, <https://doi.org/10.1093/bioinformatics/btx180>.
- [58] M. Doube, M.M. Klosowski, I. Arganda-Carreras, F.P. Cordelières, R. P. Dougherty, J.S. Jackson, B. Schmid, J.R. Hutchinson, S.J. Shefelbine, BoneJ: Free and extensible bone image analysis in ImageJ, *Bone J.* 47 (6) (2010) 1076–1079, <https://doi.org/10.1016/j.bone.2010.08.023>.
- [59] MATLAB (2020). version 9.9.0 (R2020b). Natick, Massachusetts: The MathWorks Inc.
- [60] W.L. Roque, R.R.A. Costa, A plugin for computing the pore/grain network tortuosity of a porous medium from 2D/3D MicroCT image, *Appl. Comput. Geosci.* 5 (August 2019) (2020) 100019, <https://doi.org/10.1016/j.acags.2020.100019>.
- [61] C.A. Schneider, W.S. Rasband, K.W. Eliceiri, NIH Image to ImageJ: 25 years of image analysis, *Nat. Methods* 9 (7) (2012) 671–675, <https://doi.org/10.1038/nmeth.2089>.
- [62] M.B. Dwaikat, V.K.R. Kodur, Hydrothermal model for predicting fire-induced spalling in concrete structural systems, *Fire Saf. J.* 44 (3) (2009) 425–434, <https://doi.org/10.1016/j.firesaf.2008.09.001>.
- [63] M.R. Bangi, T. Horiguchi, Pore pressure development in hybrid fibre-reinforced high strength concrete at elevated temperatures, *Cem. Concr. Res.* 41 (11) (2011) 1150–1156, <https://doi.org/10.1016/j.cemconres.2011.07.001>.
- [64] G. Choe, G. Kim, M. Yoon, E. Hwang, J. Nam, N. Guncunski, Effect of moisture migration and water vapor pressure build-up with the heating rate on concrete spalling type, *Cem. Concr. Res.* 116 (August 2017) (2019) 1–10, <https://doi.org/10.1016/j.cemconres.2018.10.021>.
- [65] Y. Li, E.H. Yang, A. Zhou, T. Liu, Pore pressure build-up and explosive spalling in concrete at elevated temperature: A review, *Constr. Build. Mater.* (2021) 284, <https://doi.org/10.1016/j.conbuildmat.2021.122818>.
- [66] P. Kalifa, F.D. Menneteau, D. Quenard, Spalling and pore pressure in HPC at high temperatures, *Cem. Concr. Res.* 30 (12) (2000) 1915–1927, [https://doi.org/10.1016/S0008-8846\(00\)00384-7](https://doi.org/10.1016/S0008-8846(00)00384-7).
- [67] T. Morita, A. Nishida, H. Hashida, N. Yamazaki, An Experimental Study on Improvement of Spalling Behavior of High-Strength Concrete Elements Under Fire Attack, *J. Struct. Constr. Eng. (Trans. AIJ)* 66 (544) (2001) 171–178, <https://doi.org/10.3130/aijs.66.171.3>.
- [68] F. Lo Monte, R. Felicetti, Heated slabs under biaxial compressive loading: a test setup for the assessment of concrete sensitivity to spalling, *Mater. Struct. /Mater. Et. Constr.* 50 (4) (2017) 1–12, <https://doi.org/10.1617/s11527-017-1055-1>.
- [69] H. Qin, J. Yang, K. Yan, J.H. Doh, K. Wang, X. Zhang, Experimental research on the spalling behaviour of ultra-high performance concrete under fire conditions, *Constr. Build. Mater.* 303 (April) (2021) 124464, <https://doi.org/10.1016/j.conbuildmat.2021.124464>.
- [70] Y. Zhang, L. Fang, S. Wu, S. Du, J. Zhang, Time dependency and similarity of gas permeability of concrete in simulated environment, *J. Build. Eng.* 51 (September 2021) (2022) 104253, <https://doi.org/10.1016/j.jobee.2022.104253>.
- [71] D. Liu, B. Savija, G.E. Smith, P.E.J. Flewitt, T. Lowe, E. Schlangen, Towards understanding the influence of porosity on mechanical and fracture behaviour of quasi-brittle materials: experiments and modelling, *Int. J. Fract.* 205 (1) (2017) 57–72, <https://doi.org/10.1007/s10704-017-0181-7>.
- [72] F. Soltani, M. Goueygou, Z. Lafhaj, B. Piwakowski, Relationship between ultrasonic Rayleigh wave propagation and capillary porosity in cement paste with variable water content, *NDT E Int.* 54 (2013) 75–83, <https://doi.org/10.1016/j.ndteint.2012.12.003>.
- [73] I. Hager, T. Tracz, M. Choinška, K. Mróz, Effect of cement type on the mechanical behavior and permeability of concrete subjected to high temperatures, *Materials* 12 (18) (2019), <https://doi.org/10.3390/ma12183021>.
- [74] A.P. Luz, M.A.L. Braulio, V.C. Pandolfelli, *Refractory Castable Engineering. F.I.R. E. Compendium series*, Goller Verl. isbn (2015), 9783872640048.
- [75] M. Maier, M. Zeiml, R. Lackner, On the effect of pore-space properties and water saturation on explosive spalling of fire-loaded concrete, *Constr. Build. Mater.* 231 (2020) 117150, <https://doi.org/10.1016/j.conbuildmat.2019.117150>.
- [76] W. Khaliq, F. Waheed, Mechanical response and spalling sensitivity of air entrained high-strength concrete at elevated temperatures, *Constr. Build. Mater.* 150 (2017) 747–757, <https://doi.org/10.1016/j.conbuildmat.2017.06.039>.
- [77] Y.S. Heo, J.G. Sanjayan, C.G. Han, M.C. Han, Relationship between inter-aggregate spacing and the optimum fibre length for spalling protection of concrete in fire, *Cem. Concr. Res.* 42 (3) (2012) 549–557, <https://doi.org/10.1016/j.cemconres.2011.12.002>.
- [78] Y. Li, P. Pimienta, N. Pinoteau, K.H. Tan, Effect of aggregate size and inclusion of polypropylene and steel fibres on explosive spalling and pore pressure in ultra-high-performance concrete (UHPC) at elevated temperature, *Cem. Concr. Compos.* 99 (January) (2019) 62–71, <https://doi.org/10.1016/j.cemconcomp.2019.02.016>.
- [79] M. Wu, J. Wu, J. Wu, B.X. Hu, A three-dimensional model for quantification of the representative elementary volume of tortuosity in granular porous media, *J. Hydrol.* 557 (2018) 128–136, <https://doi.org/10.1016/j.jhydrol.2017.12.030>.
- [80] N. Algoroudin, P. Pliya, A.-L. Beaucour, A. Simon, A. Noumowé, Influence of polypropylene and steel fibres on thermal spalling and physical-mechanical properties of concrete under different heating rates, *Constr. Build. Mater.* 259 (2020) 119690, <https://doi.org/10.1016/j.conbuildmat.2020.119690>.
- [81] Y. Ding, C. Zhang, M. Cao, Y. Zhang, C. Azevedo, Influence of different fibres on the change of pore pressure of self-consolidating concrete exposed to fire, *Constr. Build. Mater.* 113 (2016) 456–469, <https://doi.org/10.1016/j.conbuildmat.2016.03.070>.
- [82] Y.S. Heo, J.G. Sanjayan, C.G. Han, M.C. Han, Critical parameters of nylon and other fibres for spalling protection of high strength concrete in fire, *Mater. Struct.* 44 (2011) 599–610, <https://doi.org/10.1617/s11527-010-9651-3>.
- [83] G. Debicki, R. Haničič, F. Delhomme, An experimental method for assessing the spalling sensitivity of concrete mixture submitted to high temperature, *Cem. Concr. Compos.* 34 (8) (2012) 958–963, <https://doi.org/10.1016/j.cemconcomp.2012.04.002>.
- [84] EN 1992-1-1:2004; Eurocode 2: Design of concrete structures – Part 1-1: General rules and rules for buildings. European Committee for Standardization: Brussels, Belgium, 2004.
- [85] T. Uygunoğlu, I.B. Topcu, Thermal expansion of self-consolidating normal and lightweight aggregate concrete at elevated temperature, *Constr. Build. Mater.* 23 (9) (2009) 3063–3069, <https://doi.org/10.1016/j.conbuildmat.2009.04.004>.
- [86] L. Bostrom, U. Wickström, B. Ad-Zarrabi, Effect of specimen size and loading conditions on spalling of concrete, *Fire Mater.* 31 (2007) 173–186, <https://doi.org/10.1002/fam.931>.
- [87] I. Rickard, C. Maluk, L. Bisby, S. Deeny, Predictive testing for heat-induced spalling of concrete. *Structural Engineering: Providing Solutions to Global Challenges*, IABSE, Geneva, Switz. (2015), <https://doi.org/10.2749/genève.2015>.
- [88] F.P. Figueiredo, S.S. Huang, H. Angelakopoulos, K. Pilakoutas, I. Burgess, Effects of Recycled Steel and Polymer Fibres on Explosive Fire Spalling of Concrete, *Fire Technol.* 55 (2019) 1495–1516, <https://doi.org/10.1007/s10694-019-00817-9>.
- [89] F.F.M. Filho, C.R. Rodriguez, E. Schlangen, C. opuroğlu, O. Surface effects of molten slag spills on calcium aluminate cement paste, *Mater. Des.* 217 (2022) 110623, <https://doi.org/10.1016/j.matdes.2022.110623>.
- [90] M. Maier, A. Saxer, K. Bergmeister, R. Lackner, An experimental fire-spalling assessment procedure for concrete mixtures, *Constr. Build. Mater.* 232 (2020) 117172, <https://doi.org/10.1016/j.conbuildmat.2019.117172>.
- [91] M.B. Dwaikat, V.K.R. Kodur, Fire induced spalling in high strength concrete beams, *Fire Technol.* 46 (1) (2010) 251–274, <https://doi.org/10.1007/s10694-009-0088-6>.
- [92] H. Carré, P. Pimienta, C. La Borderie, F. Pereira, J.C. Mindeguia, Effect of compressive loading on the risk of spalling, *MATEC Web Conf.* 6 (2013) 1–9, <https://doi.org/10.1051/mateconf/201303061007>.

- [93] C. Kahanji, F. Ali, A. Nadjai, Explosive spalling of ultra-high performance fibre reinforced concrete beams under fire, *J. Struct. Fire Eng.* 7 (4) (2016) 328–348, <https://doi.org/10.1108/JSFE-12-2016-023>.
- [94] T.M. Jeyashree, P.R. Kannan Rajkumar, K.S. Satyanarayanan, Developments and research on fire response behaviour of prestressed concrete members – A review, *J. Build. Eng.* 57 (February) (2022) 104797, <https://doi.org/10.1016/j.jobe.2022.104797>.
- [95] PIARC – World Road Association (2016). Experience with significant incidents in road tunnels. Technical Report 2016 R35. Retrieved from <http://www.piarc.org>.
- [96] Bergmeister, K., & Francesconi, S. (2004). Causes and Frequency of Incidents in Tunnels. 5th Framework Programme of the European Union Competitive and Sustainable Growth, 1–20, Trento, Italy.
- [97] Y.Z. Li, H. Ingason, Overview of research on fire safety in underground road and railway tunnels, *Tunn. Undergr. Space Technol.* 81 (August) (2018) 568–589, <https://doi.org/10.1016/j.tust.2018.08.013>.
- [98] R. Ren, H. Zhou, Z. Hu, S. He, X. Wang, Statistical analysis of fire accidents in Chinese highway tunnels 2000–2016, *Tunn. Undergr. Space Technol.* 83 (December 2017) (2019) 452–460, <https://doi.org/10.1016/j.tust.2018.10.008>.
- [99] N. Casey, Fire incident data for Australian road tunnels, *Fire Saf. J.* 111 (November 2018) (2020) 102909, <https://doi.org/10.1016/j.firesaf.2019.102909>.
- [100] Y.S. Heo, J.G. Sanjayan, C.G. Han, M.C. Han, Synergistic effect of combined fibres for spalling protection of concrete in fire, *Cem. Concr. Res.* 40 (10) (2010) 1547–1554, <https://doi.org/10.1016/j.cemconres.2010.06.011>.
- [101] P. Ren, X. Hou, V.K.R. Kodur, C. Ge, Y. Zhao, W. Zhou, Modeling the fire response of reactive powder concrete beams with due consideration to explosive spalling, *Constr. Build. Mater.* 301 (2021) 124094, <https://doi.org/10.1016/j.conbuildmat.2021.124094>.